Available online at www.sciencedirect.com

ScienceDirect

Chinese Journal of Aeronautics 23(2010) 283-289

Chinese Journal of Aeronautics

www.elsevier.com/locate/cja

Nonlinear Stability of Supersonic Nonparallel Boundary Layer Flows

Guo Xin, Tang Dengbin*

Department of Aerodynamics, Nanjing University of Aeronautics and Astronautics, Nanjing 210016, China

Received 28 April 2009; accepted 23 August 2009

Abstract

This article studies the nonlinear evolution of disturbance waves in supersonic nonparallel boundary layer flows by using nonlinear parabolic stability equations (NPSE). An accurate numerical method is developed to solve the equations and march the NPSE in a stable manner. Through computation, are obtained the curves of amplitude and disturbance shape function of harmonic waves. Especially are demonstrated the physical characteristics of nonlinear stability of various harmonic waves, including instantaneous stream wise vortices, spanwise vortices and Λ structure etc, and are used to study and analyze the mechanism of the transition process. The calculated results have evidenced the effectiveness of the proposed NPSE method to research the nonlinear stability of the supersonic boundary layers.

Keywords: boundary layer stability; nonlinearity; supersonic flow; nonparallelism; nonlinear parabolic stability equations

1. Introduction

Closely related to the determination of the transition location and the control of boundary layers, the stability and transition of boundary layer flows are of critical importance during designing the aerial vehicles. With the dramatic development of the aeronautics and astronautics over recent years, more and more attention has been paid to the stability and the transition of supersonic boundary layer flows. Researches on stability, especially, on nonlinear stability proved very difficult to pursue because of the violent variation of many influencing parameters and acute interactions in supersonic boundary layer flows[1].

The stability theory has long been adopted to study disturbance evolution in boundary layers. As the linear parallel stability theory commonly ignores the nonparallel and the nonlinear effects[2-3], the obtained results are generally somewhat different from the reality. As a result, many methods, which consider either of the two effects, are put forward. Till now, the direct numerical simulation (DNS) of Navier-Stokes equations[4-5] seems the most powerful technique to deal with the stability phenomena, for it can simulate the whole transition process. However, the laborious computation bars it from finding wider application. Another method of parabolic stability equations (PSE)[6], which considers both the nonparallel and the nonlinear effects and dramatically decreases the time spent on computation has now replaced the PSE as a high-efficiency numerical simulation method. It has been successfully applied to the study of different stability problems, from the parallel linear to the nonparallel and nonlinear stability[7], and from the incompressible to the compressible boundary layer flows[8-9].

The nonlinear stability among various harmonic waves is the important stage in the transition process[10], and its effects manifest themselves in two ways. First, the Tollmien-Schlichting (T-S) traveling waves transform from the initial sine waves to complex waves, and the high-order wave can be obtained by using the fast Fourier transformation (FFT). Second, the traveling waves with different frequencies and spanwise cycles interact with each other. The efficient method to tackle this kind of disturbances is to decompose them into the strong fundamental mode (T-S waves) and the weak high-order mode. With the amplitude of the high-order mode gradually increasing to reach the same order as that of the fundamental mode, the periodicity is no longer obvious, and the flows enter the turbulent state.

According to the stability theory, the instability starts in the form of two-dimensional (2D) disturbances and then develops into three-dimensional (3D) disturbances[11]. The second phase of instability of 3D

*Corresponding author. Tel.: +86-25-84892624.
E-mail address: tangdbin@163.com
Foundation items: National Natural Science Foundation of China (10772082); Doctoral Foundation of Ministry of Education of China (20070287005)

doi: 10.1016/S1000-9361(09)60217-X

subharmonic disturbances is the main way of the transition. T. Herbert suggested that 3D disturbances are caused by the parameter resonance[12]. The amplitude of 3D disturbances has already become unstable even though the amplitude of the T-S waves is still low. This article focuses on the nonlinear stability of the 3D subharmonic waves, the T-S waves and their induced high-order waves in supersonic boundary layer flows.

2. Governing Equations

Decompose the instantaneous flow into laminar flow and disturbances, and insert both into the 3D unsteady compressible Navier-Stokes equations. The obtained disturbance equations are then written in the following nondimensional matrix form[13]:

$$\boldsymbol{\Gamma}^{\mathrm{l}}\frac{\partial\boldsymbol{\phi}}{\partial t}+\boldsymbol{A}^{\mathrm{l}}\frac{\partial\boldsymbol{\phi}}{\partial x}+\boldsymbol{B}^{\mathrm{l}}\frac{\partial\boldsymbol{\phi}}{\partial y}+\boldsymbol{C}^{\mathrm{l}}\frac{\partial\boldsymbol{\phi}}{\partial z}+\boldsymbol{D}^{\mathrm{l}}\boldsymbol{\phi}-\boldsymbol{V}_{xx}^{\mathrm{l}}\frac{\partial^2\boldsymbol{\phi}}{\partial x^2}-\boldsymbol{V}_{xy}^{\mathrm{l}}\frac{\partial^2\boldsymbol{\phi}}{\partial x\partial y}-\boldsymbol{V}_{yy}^{\mathrm{l}}\frac{\partial^2\boldsymbol{\phi}}{\partial y^2}-\boldsymbol{V}_{xz}^{\mathrm{l}}\frac{\partial^2\boldsymbol{\phi}}{\partial x\partial z}-\boldsymbol{V}_{yz}^{\mathrm{l}}\frac{\partial^2\boldsymbol{\phi}}{\partial y\partial z}-\boldsymbol{V}_{zz}^{\mathrm{l}}\frac{\partial^2\boldsymbol{\phi}}{\partial z^2}=\boldsymbol{F}^{\mathrm{n}} \tag{1}$$

where the disturbance $\boldsymbol{\phi}=[\rho\ u\ v\ w\ T]^{\mathrm{T}}$, $\boldsymbol{F}^{\mathrm{n}}$ is term of nonlinear interaction, and the coefficient matrices, which are $\boldsymbol{\Gamma}^{\mathrm{l}}$, $\boldsymbol{A}^{\mathrm{l}}$, $\boldsymbol{B}^{\mathrm{l}}$, $\boldsymbol{C}^{\mathrm{l}}$, $\boldsymbol{D}^{\mathrm{l}}$, $\boldsymbol{V}_{xx}^{\mathrm{l}}$, $\boldsymbol{V}_{xy}^{\mathrm{l}}$, $\boldsymbol{V}_{yy}^{\mathrm{l}}$, $\boldsymbol{V}_{xz}^{\mathrm{l}}$, $\boldsymbol{V}_{yz}^{\mathrm{l}}$ and $\boldsymbol{V}_{zz}^{\mathrm{l}}$, contain the nonparallel terms, and superscript "l" denotes the linear terms.

By using the FFT, $\boldsymbol{\phi}$ can be expressed by the following summation:

$$\boldsymbol{\phi}=\sum_{m=-\infty}^{+\infty}\sum_{n=-\infty}^{+\infty}\boldsymbol{\psi}_{m,n}\ \chi_{m,n} \tag{2}$$

where $\boldsymbol{\psi}_{m,n}=[\hat{\rho}\ \hat{u}\ \hat{v}\ \hat{w}\ \hat{T}]_{m,n}^{\mathrm{T}}$ is the disturbance shape function; $\chi_{m,n}=\exp[\mathrm{i}(\int_{x_0}^{x}\alpha_{m,n}\mathrm{d}x+n\beta z-m\omega t)]$ the wave-like function; $\alpha_{m,n}$ the streamwise wave number; $n\beta$ the spanwise wave number and $m\omega$ the angular frequency of the harmonic wave (m,n).

According to the hypothesis of PSE, the streamwise second derivatives and the products of the first derivatives of these shape functions are sufficiently small to be neglected. By applying the disturbance equations, the nonlinear parabolic stability equations (NPSE) for a random harmonic wave (m,n) can be written as

$$\hat{\boldsymbol{D}}_{m,n}\boldsymbol{\psi}_{m,n}+\hat{\boldsymbol{A}}_{m,n}\frac{\partial\boldsymbol{\psi}_{m,n}}{\partial x}+\hat{\boldsymbol{B}}_{m,n}\frac{\partial\boldsymbol{\psi}_{m,n}}{\partial y}-\boldsymbol{V}_{yy}^{\mathrm{l}}\frac{\partial^2\boldsymbol{\psi}_{m,n}}{\partial y^2}=\frac{[\boldsymbol{F}^{\mathrm{n}}]_{m,n}}{\chi_{m,n}} \tag{3}$$

where $\hat{\boldsymbol{D}}_{m,n}$, $\hat{\boldsymbol{A}}_{m,n}$ and $\hat{\boldsymbol{B}}_{m,n}$ are coefficient matrices. The terms on the left of the equation are linear[13] while those on the right nonlinear, which will be treated later.

3. Numerical Methods

Considering the ever-growing boundary layer and the rapidly changing flow field near the wall, is adopted the new curve coordinate system (ξ,η) in the streamwise and the normal direction, which is correlated to the triangle curve coordinate by

$$\left.\begin{aligned}\xi&=x\\ \eta&=\frac{c_2 y/\delta}{c_1+y/\delta}\end{aligned}\right\} \tag{4}$$

where δ is the local boundary layer thickness and c_1 and c_2 are the control parameters for mesh distribution. Thus the transformed NPSE in the new coordinate system is

$$\hat{\boldsymbol{D}}_{m,n}\boldsymbol{\psi}_{m,n}+\tilde{\boldsymbol{A}}_{m,n}\frac{\partial\boldsymbol{\psi}_{m,n}}{\partial\xi}+\tilde{\boldsymbol{B}}_{m,n}\frac{\partial\boldsymbol{\psi}_{m,n}}{\partial\eta}-(\tilde{\boldsymbol{V}}_{\eta\eta})_{m,n}\frac{\partial^2\boldsymbol{\psi}_{m,n}}{\partial\eta^2}=\frac{[\boldsymbol{F}^{\mathrm{n}}]_{m,n}}{\chi_{m,n}} \tag{5}$$

where $\tilde{\boldsymbol{A}}_{m,n}$, $\tilde{\boldsymbol{B}}_{m,n}$ and $\tilde{\boldsymbol{V}}_{\eta\eta}$ are coefficient matrices.

Differentiation is made with the forth-order differential formula[9] in the normal direction at the out bound $y=y_{\max}$, that is, the accurate gradual boundary conditions and the inviscid stability equations are imposed.

3.1. Normalization condition and spatial march

As there is an unknown variable $\alpha_{m,n}$ in Eq.(5), to make its solution unique is required an additional restraint condition called the normalization condition, which makes the PSE assumption of slow variation of shape function be satisfied. For supersonic boundary layers, the maximum disturbance function of mass flux is adopted here to determine the growth rate, and the normalization condition can be written as follows:

$$\frac{\partial([\rho u]_{m,n})_{\max}}{\partial x}\cdot\frac{1}{([\rho u]_{m,n})_{\max}}=0 \tag{6}$$

where $[\rho u]_{m,n}=\bar{\rho}\hat{u}_{m,n}+\bar{u}\hat{\rho}_{m,n}$, $\bar{\rho}$ and $\bar{u}$ are density and velocity of basic flow respectively.

In the spatial marching process, the effective predict-correct and iteration methods are employed. The solutions of the current streamwise step are predicted by those of the previous step. The calculation marches stably, until the corrected complex parameter α satisfies the accuracy requirement . The correction of α is

$$[\Delta\alpha]_{m,n}=-\mathrm{i}\frac{\left[([\rho u]_{m,n})_{i+1}\right]_{\max}-\left[([\rho u]_{m,n})_{i}\right]_{\max}}{\Delta x\left[([\rho u]_{m,n})_{i}\right]_{\max}} \tag{7}$$

It should be pointed out that there are interactions occurring among various harmonic waves because of the nonlinear effects, but they all should happen simultaneously in each spatial marching step. It is only when all the corrections satisfy the precision requirements that the computation can march forward.

3.2. Analysis of nonlinear terms

The computation of nonlinear terms of Eq.(5) is

very important to find out the accurate solution of NPSE, for a nonlinear computation of one harmonic wave (m,n) should involve the solution of other harmonic waves, which affect the wave (m,n) and the values of $\boldsymbol{\psi}_{m,n}$ are complex numbers. According to the symmetry of the Fourier transformation and the physical performances, the harmonic waves with opposite frequencies and spanwise wave numbers can be expressed by

$$\left.\begin{aligned}
&A_{m,n}=A_{-m,n}=A_{m,-n}=A_{-m,-n}\\
&\boldsymbol{\psi}_{-m,n}=[\hat{\rho}_{-m,n}\ \ \hat{u}_{-m,n}\ \ \hat{v}_{-m,n}\ \ \hat{w}_{-m,n}\ \ \hat{T}_{-m,n}]=\\
&[\hat{\rho}^{+}_{m,n}\ \ \hat{u}^{+}_{m,n}\ \ \hat{v}^{+}_{m,n}\ \ \hat{w}^{+}_{m,n}\ \ \hat{T}^{+}_{m,n}]\\
&\boldsymbol{\psi}_{m,-n}=[\hat{\rho}_{m,-n}\ \ \hat{u}_{m,-n}\ \ \hat{v}_{m,-n}\ \ \hat{w}_{m,-n}\ \ \hat{T}_{m,-n}]=\\
&[\hat{\rho}_{m,n}\ \ \hat{u}_{m,n}\ \ \hat{v}_{m,n}\ \ -\hat{w}_{m,n}\ \ \hat{T}_{m,n}]\\
&\boldsymbol{\psi}_{-m,-n}=[\hat{\rho}_{-m,-n}\ \ \hat{u}_{-m,-n}\ \ \hat{v}_{-m,-n}\ \ \hat{w}_{-m,-n}\ \ \hat{T}_{-m,-n}]=\\
&[\hat{\rho}^{+}_{m,n}\ \ \hat{u}^{+}_{m,n}\ \ \hat{v}^{+}_{m,n}\ \ -\hat{w}^{+}_{m,n}\ \ \hat{T}^{+}_{m,n}]
\end{aligned}\right\}\quad(8)$$

where the superscript "+" denotes the complex conjugate and A the amplitude.

The nonlinear terms of mode (m,n) can be formulated as

$$\boldsymbol{F}^{\mathrm{n}}_{m,n}=\sum_{m_1=-\infty}^{+\infty}\sum_{n_1=-\infty}^{+\infty}\boldsymbol{N}(m_1,n_1,m_2,n_2)\chi_{m_1,n_1}\chi_{m_2,n_2}\quad(9)$$

where the $\boldsymbol{N}(m_1,n_1,m_2,n_2)$ means the nonlinear interaction of shape function between the mode (m_1,n_1) and the mode (m_2,n_2), ($m_1+m_2=m$, $n_1+n_2=n$). The nonlinear third- and higher-order terms are ignored in $\boldsymbol{F}^{\mathrm{n}}$. The existence of phase lock relations for different harmonic waves means real($\alpha_{m,n}$) = $m\alpha_{\mathrm{r}}$ (here α_{r} is the half of the streamwise wave number of the T-S wave, $\alpha_{\mathrm{r}}=\alpha_{\mathrm{TS}}/2$). Therefore, the term on the right of Eq.(5) can be written into

$$\frac{[\boldsymbol{F}^{\mathrm{n}}]_{m,n}}{\chi_{m,n}}=\sum_{m_1=-\infty}^{+\infty}\sum_{n_1=-\infty}^{+\infty}\boldsymbol{N}(m_1,n_1,m_2,n_2)\frac{A_{m_1,n_1}A_{m_2,n_2}}{A_{m,n}}\quad(10)$$

where $A_{m,n}=A_0\exp(\int_{x_0}^{x}-\mathrm{imag}(\alpha_{m,n})\mathrm{d}x)$ is the amplitude of the harmonic wave (m_1,n_1), and A_0 the initial amplitude. The nonlinear interaction factors $\boldsymbol{N}(m_1,n_1,m_2,n_2)$ of the harmonic waves are shown in Appendix A.

4. Results and Analysis

As examples, studies have been conducted of the nonlinear interactions among various waves in the supersonic flat plate boundary layers including the 2D T-S wave (2,0) with given amplitude, the 3D subharmonic wave (1,1) with nondimensional frequency F and nondimensional spanwise wave number b, and induced high-order harmonic waves. In addition, the nonlinear growth of various waves and the physical characteristics have been analyzed. The F and b are assumed to be $10^6\omega/R_0$ and $10^3\omega/R_0$ respectively in the examples.

Fig.1 shows the spatial amplitude evolution of the 2D T-S wave (2,0) and the 3D subharmonic wave (1,1) for Ma =1.6, T_0 = 311K, F_{TS}=50, F_{sub}=25, b_{sub}= 0.053, and the initial amplitude of the T-S wave is 3%. The calculated results represented by solid lines evince a good agreement with the data from Ref.[13] represented by dots. Fig.2 shows the shape functions $|u|$ and $|T|$ of a sub- harmonic wave for Ma = 4.5, F_{TS} = 40, b_{sub}= 0.047 89 and Re = 1 500. The comparison displays a good consistency exists between the calculated results of NPSE and the data with the accurate DNS method[14] .

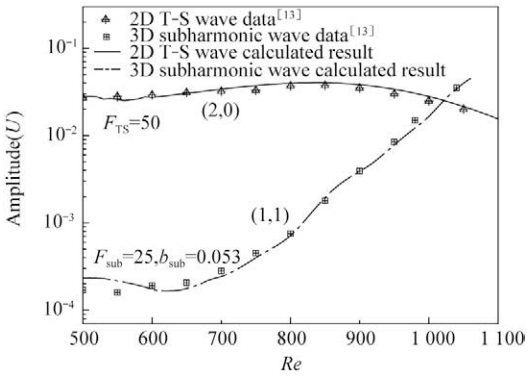

Fig.1 Amplitude evolution of modes (1,1) and (2,0).

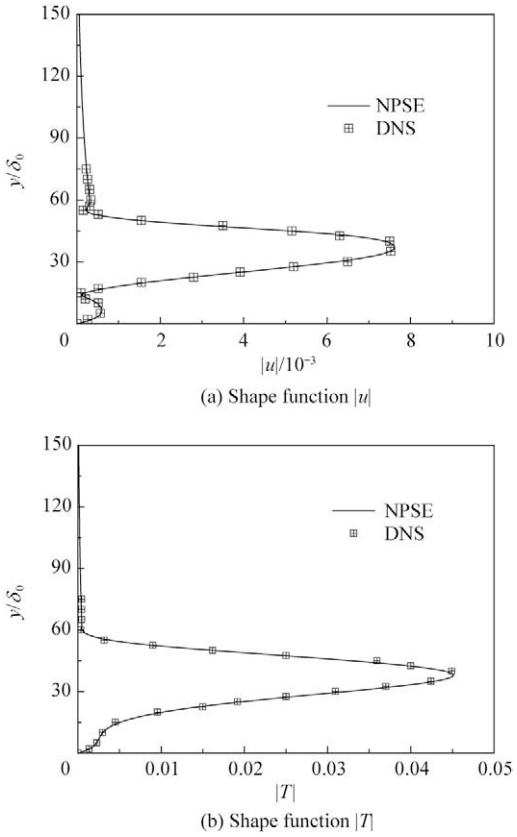

Fig.2 Comparison of disturbance shape functions.

Fig.3 illustrates the evolution curves of the T-S wave and the subharmonic waves with different initial amplitudes at Ma = 3.0. The frequency of the T-S wave

is F_{TS} = 80 and the span wise wave number of the subharmonic waves b_{sub} = 0.1. The modes of nonlinear effects on the T-S wave are (1,1) and (1,–1), and modes of nonlinear effects on the subharmonic waves are (2,0) and (–1, 1). The modes (1,–1) and (–1, 1) can be obtained by using the symmetry of FFT; therefore, the results of the modes with positive frequencies and spanwise wave numbers only need to be stored during the computation. Initial amplitudes of the T-S wave A_{0TS} are 0.5%, 0.8% and 1.0%, respectively. The corresponding initial amplitudes of the subharmonic waves are 0.005%, 0.005% and 0.05%, respectively. The spatial march starts at *Re* = 300, and initial conditions imposed are the results of linear PSE. The dash lines denote the linear PSE evolution. As seen from Fig.3, the nonlinear effects of the mode (2,0) on (1,1) appear immediately, and the growth rate larger than that of linear PSE (LPSE) because the initial amplitude of the T-S wave is much larger than that of the mode (1,1). However, the nonlinear effects of the mode (1,1) on (2,0) are insignificant except when the amplitude of the subharmonic wave becomes high enough and the difference of amplitude growth between NPSE and LPSE very small at a long initial stage. This also shows the feasibility of the linear stability theory in the early stage of the transition. With the increment of *Re*, the amplitude of mode (1,1) grows rapidly and then surpasses that of mode (2,0). As the amplitude achieves some critical value, the nonlinear effects of mode (1,1) on the T-S wave would become so significant as to prompt the amplitude of the T-S wave to change from dwindling into augmenting. When the T-S and subharmonic waves enter into the fully nonlinear stage, the amplitude of disturbances would increase quickly to reach transition. With the growth of the initial amplitude of the T-S wave, the position, where the amplitude of subharmonic wave surpasses that of the T-S wave, shifts forward, and the Reynolds number for entering the fully nonlinear stage declines gradually.

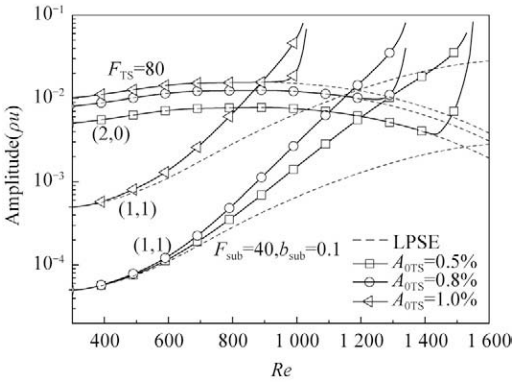

Fig.3 Amplitude evolution of modes (1,1) and (2,0) with different initial amplitudes (*Ma*=3.0).

Fig.4 illustrates the amplitude evolution of various waves, including mode (2,0), (1,1) and high-order harmonic waves at *Ma* = 3.0. The initial amplitudes of the T-S wave in Fig.4(a) and Fig.4(b) are 0.5% and 0.25% respectively. The changing trend of the amplitude of the T-S waves and subharmonic waves are the same as those in Fig.3. The high-order harmonic waves, which are induced by the nonlinear interaction, grow fast (see Fig.4(a)). The amplitude of mode (2,2) mainly induced by (1,1) grows rapidly from *Re* = 830. At a short distance, the amplitude grows by a factor of 10 000 reaching that of the T-S wave. The rapid increase of the amplitude of mode (4,2) appears at *Re* = 980. With the amplitude growing, the nonlinear effects become stronger and stronger and finally, persuade the amplitudes of all harmonic waves to reach a higher level. Fig.4(b) differentiates from Fig.4(a) in that the initial amplitude of the T-S wave is so low that it makes the subharmonic waves unable to grow enough, and it itself appears to increase slowly and then decreases, actually, not entering the nonlinear stage. Similarly, the amplitudes of the high-order harmonic waves fail to go up to a high level too.

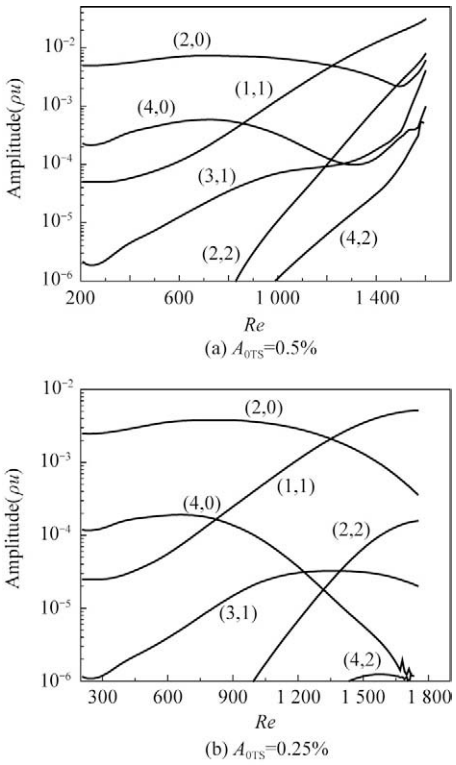

Fig.4 Amplitude evolution of various harmonic waves.

Fig.5 discloses the nonlinear evolution of the amplitude of the second mode fundamental wave[15] with F_{TS} = 240 and the corresponding subharmonic wave with F_{sub}=120, b_{sub}= 0.2 at *Ma* = 6.0. The amplitudes of T-S wave are 0.5%, 0.8% and 0.1%, respectively. The dash and solid lines evince the results of LPSE and NPSE, respectively. Similar to Fig.3, with the increment of the initial amplitude of the T-S wave, the nonlinear effects on the subharmonic waves strengthen gradually, and the position for them to enter nonlinear stage shifts forward. As the amplitude of T-S waves is

small enough (for instance 0.001), the evolution of subharmonic waves is at linear stage at $300 < Re < 720$, but the T-S wave evolves all the time at the linear stage.

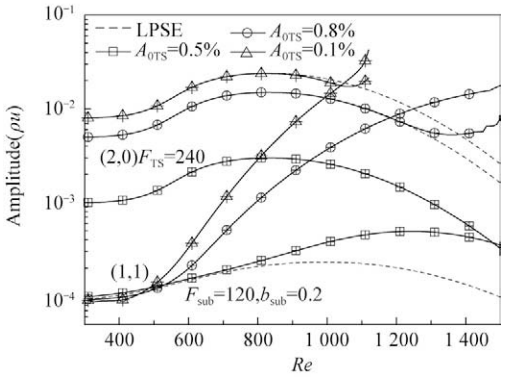

Fig.5 Amplitude evolution of modes (1,1) and (2,0) with different initial amplitudes (*Ma*=6.0).

In Fig.6, the streamlines in *yz* plane at different streamwise positions with the same phase angle display clearly the formation and the evolution of the streamwise vortices. At the position *y*=15, the crossings appear (see Fig.6(a)) and then streamwise gradually scatter (see Fig.6(b)) with vortex-centers forming (see Fig.6(c)). Finally, a couple of vortices form in mutually opposite directions (see Fig.6(d)).

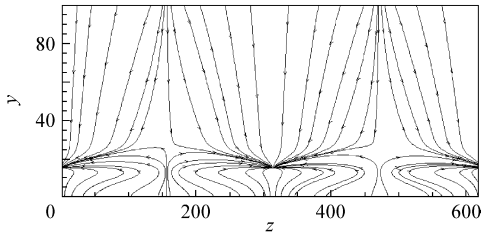

(a) *Re*=783

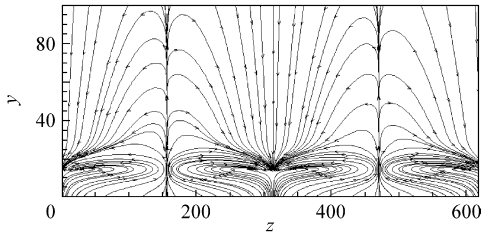

(b) *Re*=840

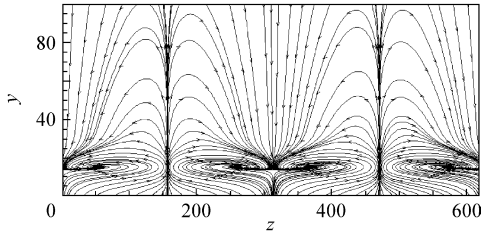

(c) *Re*=870

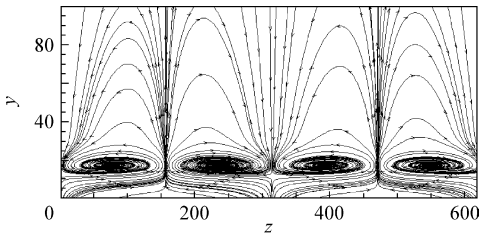

(d) *Re*=926

Fig.6 Streamlines on *yz* plane at different streamwise positions.

Fig.7 shows the spanwise vortex contours in *xy* plane with different spanwise phase angles for *Ma*=3.0, F_{TS}=80, and b_{sub}=0.1. The initial amplitude of the T-S wave is 1.0% and that of the subharmonic wave 0.05%. With the streamwise marching, the closed spanwise vortices take form with dimensions expanding, and the normal positions of vortex center rising (see Fig.7(a)). As the amplitude of the 3D subharmonic wave increases, the amplitude of the T-S wave attains 6% and that of the subharmonic wave 2% at about *x*=5 000 (*Re*=1 000) (see Fig.3), and the spanwise vortices evolve into many small-size vortices. The phase angle π/2 is the neutral position of 3D disturbances (see Fig.7(b)), where the 3D disturbance value is zero with the mere existence of T-S wave. The distance between the centers of the neighboring vortices is

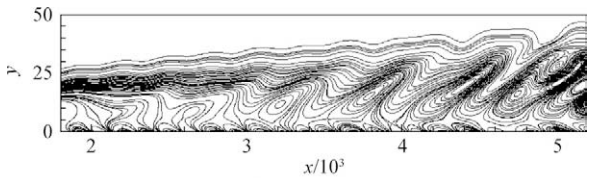

(a) Phase angle is 0

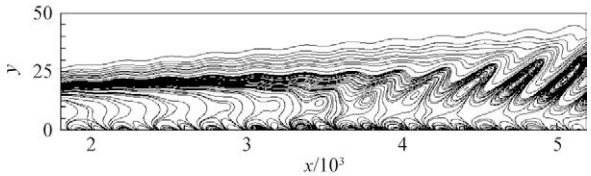

(b) Phase angle is π/2

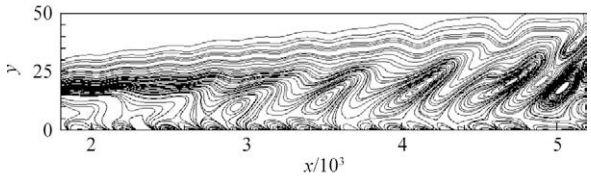

(c) Phase angle is π

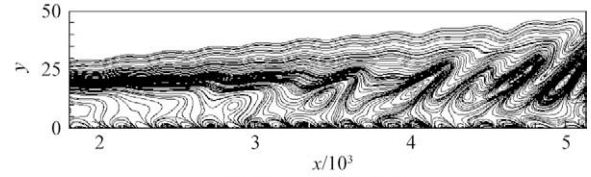

(d) Phase angle is 2π/3

Fig.7 Contours of spanwise vortices.

about 300 (i.e. the wave length of the T-S wave), signifying approximately an invariance streamwise. Fig.7(a) displays the peaks and Fig.7(c) the troughs of the subharmonic waves. The distance between the centers of the neighboring vortices induced by the combined reaction of both waves is about 600 (i.e. the streamwise wave length of the subharmonic wave). In Fig.7(d), the amplitudes of the 3D subharmonic waves are half of those in Fig.7(a). The small vortices that happen between two large vortices at about x= 4 400 also stem from the combined reactions of both waves.

As an important characteristic of the subharmonic instability, the formation of the staggered Λ structure is called H-type instability[16]. Fig.8 shows the plots of the instantaneous velocity contours with the same computational parameters as those in Fig.4(a). The normal position is y/δ_0=65 (Re_{δ_0} = 200). As the amplitude of subharmonic waves grows to a certain value, the staggered contour structures present themselves in Fig.8 with their corresponding instantaneous contour floods of the total vortices in Fig.9, where the Λ structures cannot be too clearly observed (in Fig.9, the darker the color, the bigger the value of vortices), which leads to final breakdown and transition of flows.

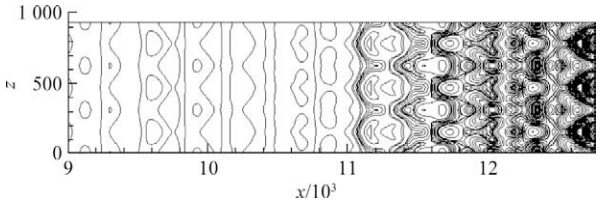

Fig.8 Contours of instantaneous velocity u.

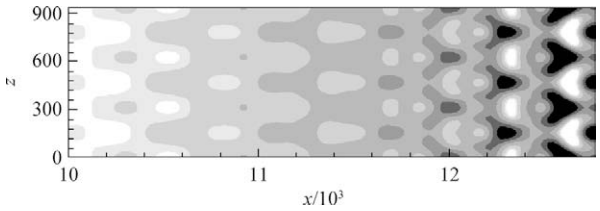

Fig.9 Contour floods of instantaneous total vortices.

5. Conclusions

This article proposes the NPSE to study the nonparallel and nonlinear supersonic boundary layer stability. The results show that in the 2D T-S periodical disturbances with finite amplitudes, the nonlinear interactions prompt the amplitude of 3D disturbances and high-order harmonic waves to grow fast. The nonlinear evolution of the streamwise and the spanwise vortices and the Λ structures that are clearly picturized by figures are used to analyze the transition processes. This makes the computational cost much lower than that if DNS of Navier-Stokes equations is adopted. Therefore, the proposed NPSE is evidenced to be a powerful tool in studying the nonlinear stability in supersonic boundary layer flow.

References

[1] Fasel H F, Thumm A. Numerical simulation of three-dimensional break down in supersonic boundary layer transition. American Physical Society 1991; 36:2701.
[2] Smith F T. On the non-parallel flow stability of the Blasius boundary layer. Proceedings of the Royal Society of London, Series A—Mathematical and Physical Sciences 1979; 366(1724): 91-109.
[3] El-Hady N M. Nonparallel instability of supersonic and hypersonic boundary layers. AIAA-1991-324, 1991.
[4] Joslin R D, Streett C L, Chang C L. Spatial direct numerical simulation of boundary-layer transition mechanisms: validation of PSE theory. Theoretical and Computational Fluid Dynamics 1993; 4(6): 271-288.
[5] Zhang L, Tang D B. Nonlinear evolution of turbulent spots in the near-wall shear flow. Science in China: Series G: Physics Mechanics and Astronomy 2006; 49(2): 158-168.
[6] Herbert T. Parabolized stability equations. Annual Review of Fluid Mechanics 1997; 29:245-285.
[7] Bertolotti F P. Linear and nonlinear stability of boundary layers with streamwise varying properties. PhD thesis, The Ohio State University, 1991.
[8] Bertolotti F P, Herbert T. Analysis of the linear stability of compressible boundary layers using the PSE. Theoretical and Computational Fluid Dynamics 1991; 3(2): 117-124.
[9] Zhang Y M, Zhou H. PSE as applied to problems of transition in compressible boundary layers. Applied Mathematics and Mechanics 2008; 29(7): 833-840.
[10] Crouch J D, Herbert T. Nonlinear evolution of secondary instabilities in boundary-layer transition. Theoretical and Computational Fluid Dynamics 1993; 4(4): 151-175.
[11] Liu J, Tang D B, Yang Y Z. On nonlinear evolution of C-type instability in nonparallel boundary layers. Chinese Journal of Aeronautics 2007; 20:313-320.
[12] Herbert T. Secondary instability of boundary layers. Annual Review of Fluid Mech 1988; 20:487-526.
[13] Chang C L, Malik M R, Erlebacher G, et al. Linear and nonlinear PSE for compressible boundary layers. ICASE Report 93-70, 1993.
[14] Jiang L, Choudhari M, Chang C L, et al. Numerical simulations of laminar-turbulent transition in supersonic boundary layer. AIAA-2006-3224, 2006.
[15] Guo X, Tang D B, Shen Q. Boundary layer stability with multiple modes in hypersonic flows. Modern Physics Letters B(MPLB) 2009; 23(3): 321-324.
[16] Schmid P J, Henningson D S. Stability and transition in shear flows. In: Applied Mathematical Sciences. New York: Springer-Verlag, 2001.

Biography:

Guo Xin Born in 1981, he received B.S. degree from Nanjing University of Aeronautics and Astronautics in 2004. Now he is a Ph.D. candidate in the same university. His main research interest lies in computational fluid dynamics and flow stability.
E-mail: guoxincn@sina.com

Appendix A: Derivation of nonlinear interaction factor $N(m_1,n_1,m_2,n_2)$ in Eq.(10)

$$(N(m_1,n_1,m_2,n_2))_1=-(\rho_1\frac{\partial u_2}{\partial x}+\rho_1\frac{\partial v_2}{\partial y}+\rho_1\frac{\partial w_2}{\partial z}+\frac{\partial\rho_1}{\partial x}u_2+\frac{\partial\rho_1}{\partial y}v_2+\frac{\partial\rho_1}{\partial z}w_2)$$

$$(N(m_1,n_1,m_2,n_2))_2=-\frac{1}{\gamma M^2}\frac{\partial\rho_1}{\partial x}T_2-\frac{1}{\gamma M^2}\rho_1\frac{\partial T_2}{\partial x}+\frac{1}{R_0}[\frac{\mathrm{d}\overline{\mu}}{\mathrm{d}T}(\frac{\partial^2u_1}{\partial x^2}+\frac{\partial^2u_1}{\partial y^2}+\frac{\partial^2u_1}{\partial z^2})T_2+\frac{1}{3}\frac{\mathrm{d}\overline{\mu}}{\mathrm{d}T}(\frac{\partial^2u_1}{\partial x^2}+\frac{\partial^2v_1}{\partial x\partial y}+\frac{\partial^2w_1}{\partial x\partial z})T_2+$$
$$(\frac{4}{3}\frac{\partial u_1}{\partial x}-\frac{2}{3}\frac{\partial v_1}{\partial y}-\frac{2}{3}\frac{\partial w_1}{\partial z})(\frac{\mathrm{d}\overline{\mu}}{\mathrm{d}T}\frac{\partial T_2}{\partial x}+\frac{\mathrm{d}^2\overline{\mu}}{\mathrm{d}T^2}\frac{\partial\overline{T}}{\partial x}T_2)+(\frac{\partial v_1}{\partial x}+\frac{\partial u_1}{\partial y})(\frac{\mathrm{d}\overline{\mu}}{\mathrm{d}T}\frac{\partial T_2}{\partial y}+\frac{\mathrm{d}^2\overline{\mu}}{\mathrm{d}T^2}\frac{\partial\overline{T}}{\partial y}T_2)+(\frac{\partial u_1}{\partial z}+\frac{\partial w_1}{\partial x})(\frac{\mathrm{d}\overline{\mu}}{\mathrm{d}T}\frac{\partial T_2}{\partial z})]-$$
$$(\rho_1\frac{\partial u_2}{\partial t}+\frac{\partial\overline{u}}{\partial x}\rho_1u_2+\frac{\partial\overline{u}}{\partial y}\rho_1v_1+\overline{\rho}u_1\frac{\partial u_2}{\partial x}+\overline{\rho}v_1\frac{\partial u_2}{\partial y}+\overline{\rho}w_1\frac{\partial u_2}{\partial z}+\overline{u}\rho_1\frac{\partial u_2}{\partial x}+\overline{v}\rho_1\frac{\partial u_2}{\partial y})$$

$$(N(m_1,n_1,m_2,n_2))_3=-\frac{1}{\gamma M^2}\frac{\partial\rho_1}{\partial y}T_2-\frac{1}{\gamma M^2}\rho_1\frac{\partial T_2}{\partial y}+\frac{1}{R_0}[\frac{\mathrm{d}\overline{\mu}}{\mathrm{d}T}(\frac{\partial^2v_1}{\partial x^2}+\frac{\partial^2v_1}{\partial y^2}+\frac{\partial^2v_1}{\partial z^2})T_2+\frac{1}{3}\frac{\mathrm{d}\overline{\mu}}{\mathrm{d}T}(\frac{\partial^2u_1}{\partial x\partial y}+\frac{\partial^2v_1}{\partial y^2}+\frac{\partial^2w_1}{\partial y\partial z})T_2+$$
$$(\frac{\partial v_1}{\partial x}+\frac{\partial u_1}{\partial y})(\frac{\mathrm{d}\overline{\mu}}{\mathrm{d}T}\frac{\partial T_2}{\partial x}+\frac{\mathrm{d}^2\overline{\mu}}{\mathrm{d}T^2}\frac{\partial\overline{T}}{\partial x}T_2)+(-\frac{2}{3}\frac{\partial u_1}{\partial x}+\frac{4}{3}\frac{\partial v_1}{\partial y}-\frac{2}{3}\frac{\partial w_1}{\partial z})(\frac{\mathrm{d}\overline{\mu}}{\mathrm{d}T}\frac{\partial T_2}{\partial y}+\frac{\mathrm{d}^2\overline{\mu}}{\mathrm{d}T^2}\frac{\partial\overline{T}}{\partial y}T_2)+(\frac{\partial w'}{\partial y}+\frac{\partial v'}{\partial z})(\frac{\mathrm{d}\overline{\mu}}{\mathrm{d}T}\frac{\partial T'}{\partial z})]-$$
$$(\rho_1\frac{\partial v_2}{\partial t}+\frac{\partial\overline{v}}{\partial x}\rho_1u_2+\frac{\partial\overline{v}}{\partial y}\rho_1v_2+\overline{\rho}u'\frac{\partial v_2}{\partial x}+\overline{\rho}v_1\frac{\partial v_2}{\partial y}+\overline{\rho}w_1\frac{\partial v_2}{\partial z}+\overline{u}\rho_1\frac{\partial v_2}{\partial x}+\overline{v}\rho_1\frac{\partial v_2}{\partial y})$$

$$(N(m_1,n_1,m_2,n_2))_4=-\frac{1}{\gamma M^2}\frac{\partial\rho_1}{\partial y}T_2-\frac{1}{\gamma M^2}\rho_1\frac{\partial T_2}{\partial y}+\frac{1}{R_0}[\frac{\mathrm{d}\overline{\mu}}{\mathrm{d}T}(\frac{\partial^2v_1}{\partial x^2}+\frac{\partial^2v_1}{\partial y^2}+\frac{\partial^2v_1}{\partial z^2})T_2+\frac{1}{3}\frac{\mathrm{d}\overline{\mu}}{\mathrm{d}T}(\frac{\partial^2u_1}{\partial x\partial y}+\frac{\partial^2v_1}{\partial y^2}+\frac{\partial^2w_1}{\partial y\partial z})T_2+$$
$$(\frac{\partial v_1}{\partial x}+\frac{\partial u_1}{\partial y})(\frac{\mathrm{d}\overline{\mu}}{\mathrm{d}T}\frac{\partial T_2}{\partial x}+\frac{\mathrm{d}^2\overline{\mu}}{\mathrm{d}T^2}\frac{\partial\overline{T}}{\partial x}T_2)+(-\frac{2}{3}\frac{\partial u_1}{\partial x}+\frac{4}{3}\frac{\partial v_1}{\partial y}-\frac{2}{3}\frac{\partial w_1}{\partial z})(\frac{\mathrm{d}\overline{\mu}}{\mathrm{d}T}\frac{\partial T_2}{\partial y}+\frac{\mathrm{d}^2\overline{\mu}}{\mathrm{d}T^2}\frac{\partial\overline{T}}{\partial y}T_2)+(\frac{\partial w_1}{\partial y}+\frac{\partial v_1}{\partial z})(\frac{\mathrm{d}\overline{\mu}}{\mathrm{d}T}\frac{\partial T_2}{\partial z})]-$$
$$(\rho_1\frac{\partial v_2}{\partial t}+\frac{\partial\overline{v}}{\partial x}\rho_1u_2+\frac{\partial\overline{v}}{\partial y}\rho_1v_2+\overline{\rho}u_1\frac{\partial v_2}{\partial x}+\overline{\rho}v_1\frac{\partial v_2}{\partial y}+\overline{\rho}w_1\frac{\partial v_2}{\partial z}+\overline{u}\rho_1\frac{\partial v_2}{\partial x}+\overline{v}\rho_1\frac{\partial v_2}{\partial y})$$

$$(N(m_1,n_1,m_2,n_2))_5=\frac{1}{R_0\sigma}[\frac{\mathrm{d}\overline{\kappa}}{\mathrm{d}T}(\frac{\partial^2T_1}{\partial x^2}T_2+\frac{\partial T_1}{\partial x}\frac{\partial T_2}{\partial x}+\frac{\partial^2T_1}{\partial y^2}T_2+\frac{\partial T_1}{\partial y}\frac{\partial T_2}{\partial y}+\frac{\partial^2T_1}{\partial z^2}T_2+$$
$$\frac{\partial T_1}{\partial z}\frac{\partial T_2}{\partial z})+\frac{\mathrm{d}^2\overline{\kappa}}{\mathrm{d}T^2}\frac{\partial\overline{T}}{\partial x}\frac{\partial T_1}{\partial x}T_2'+\frac{\mathrm{d}^2\overline{\kappa}}{\mathrm{d}T^2}\frac{\partial\overline{T}}{\partial y}\frac{\partial T_1}{\partial y}T_2'+\frac{\mathrm{d}^2\overline{\kappa}}{\mathrm{d}T^2}\frac{\partial\overline{T}}{\partial z}\frac{\partial T_1}{\partial z}T_2']+\frac{Ec}{\gamma M^2}[\rho_1\frac{\partial T_2}{\partial t}+\frac{\partial\rho_1}{\partial t}T_2'+(\overline{\rho}\frac{\partial T_1'}{\partial x}+\frac{\partial\overline{\rho}}{\partial x}T_1+$$
$$\frac{\partial\overline{T}}{\partial x}\rho_1'+\overline{T}\frac{\partial\rho_1}{\partial x})u_2'+(\rho_1\frac{\partial T_2}{\partial x}+\frac{\partial\rho_1}{\partial x}T_2)\overline{u}+(\overline{\rho}\frac{\partial T_1}{\partial y}+\frac{\partial\overline{\rho}}{\partial y}T_1+\frac{\partial\overline{T}}{\partial y}\rho_1+\overline{T}\frac{\partial\rho_1}{\partial y})v_2+(\overline{\rho}\frac{\partial T_1}{\partial z}+\frac{\partial\overline{\rho}}{\partial z}T_1+\frac{\partial\overline{T}}{\partial z}\rho_1+\overline{T}\frac{\partial\rho_1}{\partial z})w_2]+$$
$$Ec\frac{\overline{\mu}}{R_0}[\frac{4}{3}\frac{\partial u_1}{\partial x}\frac{\partial u_2}{\partial x}+\frac{4}{3}\frac{\partial v_1}{\partial y}\frac{\partial v_2}{\partial y}+\frac{4}{3}\frac{\partial w_1}{\partial z}\frac{\partial w_2}{\partial z}+\frac{\partial v_1}{\partial x}\frac{\partial v_2}{\partial x}+\frac{\partial u_1}{\partial y}\frac{\partial u_2}{\partial y}+\frac{\partial u_1}{\partial z}\frac{\partial u_2}{\partial z}+\frac{\partial w_1}{\partial x}\frac{\partial w_2}{\partial x}+$$
$$(\rho_1\frac{\partial T_2}{\partial y}+\frac{\partial\rho_1}{\partial y}T_2)\overline{v}+\frac{\partial w_1}{\partial y}\frac{\partial w_2}{\partial y}+\frac{\partial v_1}{\partial z}\frac{\partial v_2}{\partial z}+2\frac{\partial v_1}{\partial x}\frac{\partial u_2}{\partial y}+2\frac{\partial u_1}{\partial z}\frac{\partial w_2}{\partial x}+2\frac{\partial w_1}{\partial y}\frac{\partial v_2}{\partial z}-\frac{4}{3}\frac{\partial u_1}{\partial x}\frac{\partial v_2}{\partial y}-\frac{4}{3}\frac{\partial v_1}{\partial y}\frac{\partial w_2}{\partial z}-\frac{4}{3}\frac{\partial u_1}{\partial x}\frac{\partial w_2}{\partial z}]+$$
$$\frac{Ec}{R_0}\frac{\mathrm{d}\overline{\mu}}{\mathrm{d}T}T_1[(\frac{8}{3}\frac{\partial\overline{u}}{\partial x}-\frac{4}{3}\frac{\partial\overline{v}}{\partial y})\frac{\partial u_2}{\partial x}+(-\frac{4}{3}\frac{\partial\overline{u}}{\partial x}+\frac{8}{3}\frac{\partial\overline{v}}{\partial y})\frac{\partial v_2}{\partial y}+(-\frac{4}{3}\frac{\partial\overline{u}}{\partial x}-\frac{4}{3}\frac{\partial\overline{v}}{\partial y})\frac{\partial w_2}{\partial z}+2\frac{\partial\overline{u}}{\partial y}\frac{\partial u_2}{\partial y}+2\frac{\partial\overline{u}}{\partial z}\frac{\partial u_2}{\partial z}+2\frac{\partial\overline{v}}{\partial x}\frac{\partial v_2}{\partial x}+$$
$$2\frac{\partial\overline{v}}{\partial z}\frac{\partial v_2}{\partial z}+2\frac{\partial\overline{v}}{\partial x}\frac{\partial u_2}{\partial y}+2\frac{\partial\overline{u}}{\partial y}\frac{\partial v_2}{\partial x}+2\frac{\partial\overline{u}}{\partial z}\frac{\partial w_2}{\partial x}]-\frac{\mathrm{d}\overline{c}_\mathrm{p}}{\mathrm{d}T}(\frac{\partial\overline{T}}{\partial x}\overline{u}+\frac{\partial\overline{T}}{\partial y}\overline{v})\rho_1T_2-$$
$$\overline{\rho}\frac{\mathrm{d}\overline{c}_\mathrm{p}}{\mathrm{d}T}(\frac{\partial T_1}{\partial t}+\overline{u}\frac{\partial T_1}{\partial x}+\overline{v}\frac{\partial T_1}{\partial y}+\frac{\partial\overline{T}}{\partial x}u_1+\frac{\partial\overline{T}}{\partial y}v_1)T_2-\overline{c}_\mathrm{p}(\frac{\partial T_1}{\partial t}+\overline{u}\frac{\partial T_1}{\partial x}+\overline{v}\frac{\partial T_1}{\partial y}+\frac{\partial\overline{T}}{\partial x}u_1+\frac{\partial\overline{T}}{\partial y}v_1)\rho_2$$

where the subscripts 1 denotes the mode (m_1, n_1) and 2 the mode (m_2, n_2).

$$\boldsymbol{\psi}_1=[\rho_1\ \ u_1\ \ v_1\ \ w_1\ \ T_1]^\mathrm{T},\quad \boldsymbol{\psi}_2=[\rho_2\ \ u_2\ \ v_2\ \ w_2\ \ T_2]^\mathrm{T}$$

The derivatives of $\boldsymbol{\psi}_1$ in streamwise and spanwise directions are expressed as below by taking $\boldsymbol{\psi}_1$ for example:

$$\frac{\partial\boldsymbol{\psi}_1}{\partial x}=\mathrm{i}m_1\alpha_\mathrm{r}\boldsymbol{\psi}_{m_1,n_1},\quad \frac{\partial^2\boldsymbol{\psi}_1}{\partial x^2}=-(m_1\alpha_\mathrm{r})^2\boldsymbol{\psi}_{m_1,n_1}+\mathrm{i}\cdot2m_1\alpha_\mathrm{r}\frac{\partial\boldsymbol{\psi}_{m_1,n_1}}{\partial x}+\mathrm{i}m_1\frac{\mathrm{d}\alpha_\mathrm{r}}{\mathrm{d}x}\boldsymbol{\psi}_{m_1,n_1},$$

$$\frac{\partial\boldsymbol{\psi}_1}{\partial z}=\mathrm{i}n_1\beta\boldsymbol{\psi}_{m_1,n_1},\quad \frac{\partial^2\boldsymbol{\psi}_1}{\partial z^2}=-(n_1\beta)^2\boldsymbol{\psi}_{m_1,n_1},\quad \frac{\partial\boldsymbol{\psi}_1}{\partial t}=-\mathrm{i}m_1\omega\boldsymbol{\psi}_{m_1,n_1}$$